Ferroelectric surface induced electron doping in zigzag graphene nanoribbon

G D Belletti[1], S D Dalosto[1] and Silvia Tinte[1]

[1]Instituto de Física del Litoral-CONICET, Universidad Nacional del Litoral, Güemes 3450, (3000) Santa Fe, Argentina

E-mail: silvia.tinte@santafe-conicet.gov.ar

Abstract. The interface between a zigzag graphene nanoribbon ($zGNR$) and the ferroelectric $PbTiO_3$ (001) surface is studied through first-principles calculations. We investigate how the electric polarization normal to the surface tunes the $zGNR$ electronic and magnetic properties. A ferroelectric single-domain configuration with polarization up and down is considered including explicitly a bottom metallic electrode. Our results show how not only the ferroelectric polarization direction determines the doping in $zGNR$: the downward polarization induces a p-type doping in a planar $zGNR$ whereas the upward polarization keeps it *intrinsic*; but also the features of the clean ferroelectric surface, such as the atomic relaxation and the electronic distribution. Interestingly, the surface ferroelectric polarization, besides tuning the carrier type as it does in graphene, also closes the $zGNR$ band gap which can be understood in terms of the weakening of the local magnetic moment of the edge carbon atoms as the polarization increases. The $zGNR$ antiferromagnetic ground state is preserved without breaking the α-β degeneracy.

Keywords: DFT, graphene, ferroelectrics, first principles

Submitted to: *J. Phys.: Condens. Matter*
Online supplementary data available from ???
(Some figures may appear in color only in the online journal)

1. Introduction

Graphene holds promises to revolutionize the current nanotechnology [1]. Combining graphene with different functional materials ranging from dielectrics, semiconductors, metals to organic compounds, have broadened its technological applications including novel materials, devices, sensors, catalysts, sensors, and biomedical treatments [2]. Among functional materials, ferroelectrics not only possess high dielectric constant and nonlinearity, but also exhibit non-volatile memory behavior due to their unique feature of spontaneous electric polarization. Integration of graphene with ferroelectrics has been intensively investigated mostly in the fabrication of field-effect transistors (FETs) [3, 4, 5, 6, 7], which furthermore shows a means of manipulating charge carriers in

graphene [8, 9]. For instance, deposition of graphene on a ferroelectric $Pb(Zr_{1-x}Ti_x)O_3$ thin film indicates that the ferroelectric polarization arising from the underlying PZT can control the carrier type in graphene [7] which can be tuned from p- to n-type by the polarization reversal. This displays the strong influence of the ferroelectric polarization on the electronic properties of graphene. Spatial modulation of carrier density in graphene was recently demonstrated through coupling to an adjacent distribution of ferroelectric polarization forming 180° domains in a $LiNbO_3$ substrate [10]. Periodic arrays of p-n junctions in vacuum were observed, and first-principles calculations have contributed to elucidate the interplay between graphene and the $LiNbO_3$ surface.

On the other hand, the absence of a band gap in $2D$ graphene is an undesirable requirement for the electronic industry. One of the most promising way to overcome it, is cutting graphene in $1D$ nanoribbons whose electronic properties depend on their edge termination [11]. GNRs with zigzag edges have band gap and therefore are semiconductors, but the energy gap decreases as the ribbon width increases [12, 13]. Other electrical properties such as the doping level and the Fermi energy can also be tuned. For instance, fabricated GNR-based FETs on non-ferroelectric substrate have shown that the electronic doping p-type and n-type can be obtained by functionalizing the GNR edges with oxygen [14] or nitrogen [15] species, respectively. Therefore, it seems interesting to ask how a ferroelectric polarization will affect the electronic properties of a GNR since its edges are very reactive. From the theoretical side, the nature of the interaction of a ferroelectic with graphene has been investigated [16, 10], whereas with a GNR, only the effect of ferroelectric molecules has been reported [17]. A complete description of a GNR interacting with the surface of a ferroelectric material is lacking.

In this work we combine $zGNR$s with a ferroelectric oxide focusing on the interplay of the systems at the interface. Specifically, we investigate from an atomistic point of view how the interaction of a $zGNR$ with the ferroelectric polarization of the $PbTiO_3$ (001) surface affects the electronic and magnetic properties of the nanoribbon by performing first-principles calculations. In this study, the ferroelectric presents a monodomain configuration with polarization pointing up (P^+) and down (P^-) of the surface, and also in the nonpolar state. We do not take into account the switching process itself, the surface reconstruction neither surface defects. A $zGNR$ with H-atom saturated edges is considered without reconstruction at the edges neither defects. In this way, the intrinsic effect of the ferroelectric polarization on $zGNR$ is explored. Our results indicate that both the polarization direction and the surface atomic relaxation determine the electronic charge redistribution at the interface of the hybrid system, which regulates the $zGNR$ electron doping as well as its band gap. The paper is organized as follows. Section II describes the methodology and the geometry of the hybrid system. Section III presents the results and discussions, and ends up with the conclusions.

2. Methodology and system description

We perform standard first-principles calculations using the density functional theory as implemented in the Vienna *Ab initio* Simulation Package (VASP) [18]. Collinear spin-polarized calculations using the generalized gradient approximation with the Perdew-Burke-Ernzeholf parameterization for solids (PBE-sol) [19], and including the effect of van der Waals interactions by means of the DFT-D3 method of Grimme [20] are performed. The projector augmented-wave potentials are used with 500 eV cutoff for the plane wave basis set. Convergence with respect to the k-point mesh is achieved using a $2\times1\times1$-centered grid. A Gaussian smearing of 0.1 eV is used to accelerate convergence of the Brillouin-zone integration.

A $zGNR$ terminated at the edges with hydrogen atoms is placed on a (001) surface of an ultrathin film of the ferroelectric $PbTiO_3$ (PTO) attached to a platinum electrode as seen in Figure 1. We describe first the two systems, and provide some details in the Supplementary Information, then present our results for the hybrid system.

The ferroelectric material is modeled as a slab with geometry vacuum / insulator / metal / vacuum as sketched in Figure 1(a). Our work is constrained to model PTO ultrathin films epitaxially grown with polarization only in the z-direction, perpendicular to the surface. The system is made up of $2\times4\times4.5$ PTO unit cells stacked on an electrode represented by $4 \times 4 \times 3$ Pt unit cells in a fcc(111) stacking. Both the insulator and the electrode are constrained to keep a square in-plane lattice of side length equals to the PBE-sol theoretical bulk value of tetragonal PTO: $a_{PTO} = 3.874$ Å, [21], and their x and y coordinates fixed at the high-symmetry positions since the in-plane polarization is zero. We consider TiO_2-terminated (001) PTO films both in the free surface and in the electrode side having a TiO_2-Pt interface. This surface termination was chosen based on two facts: studies on the interaction of graphene with metallic Ti [23, 24] and with TiO_2 oxide [25, 26] suggest that the stoichiometric TiO_2-terminated surface of PTO [27] would be reactive to interact with GNRs, and furthermore this surface is simpler to model than PbO-terminated one because the antiferrodistortive distortions related with the oxygen octahedron rotations can be safely neglected [28]. Periodic boundary conditions are taken along the three directions, and a 20 Å vacuum region along z-direction separates the slab from its periodic images. The standard dipole correction [29] is used to simulate open circuit boundary conditions by enforcing a zero electric field in the vacuum layer. We model PTO ultrathin films in *(i)* a nonpolar and *(ii)* two polar states: P^+ and P^- along z-direction in a monodomain configuration with the modulus of P which equals to 0.53 P_0, where $P_0 = 79\ \mu C/cm^2$ is the bulk value. This restriction is applied to avoid complications which could arise from pathological band alignments [30], due to the well-known underestimation of the DFT band gap (see Figure S1). To set a given P value, as an approximation the atoms of the two atomic layers next-nearest neighbors to the electrode interface (layers 7 and 8 in Figure 1) are displaced along z direction to reproduce P, and while they are kept fixed, the z positions of all other atoms are relaxed. In particular for the nonpolarized state, those atomic layers are separated in $c_0/2$, where

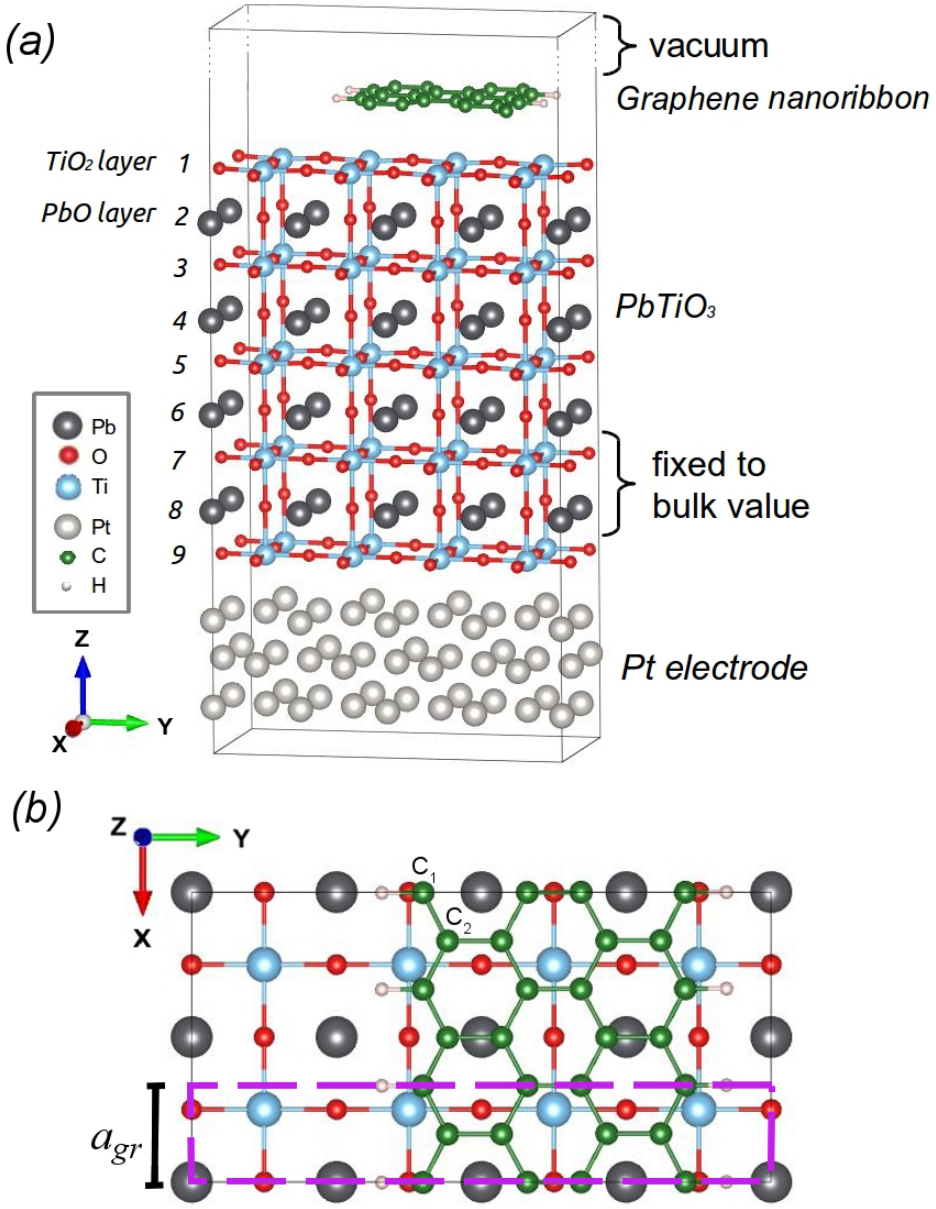

Figure 1. Schematic representation of the simulation supercell. (a) Lateral view of the full system: graphene nanoribbon over the PTO slab attached to a Pt electrode, including part of the vacuum space. (b) Top view of the TiO_2-terminated PTO surface and the stretched nanoribbon to match the PTO unit cell. Only the atoms at the surface are shown to facilitate visualization. The dashed magenta box indicates the primitive unit cell of the expanded $zGNR$ with a_{gr} the distorted lattice parameter, and the y-direction side matching the simulation supercell of the hybrid system. This unit repeated three times along x direction builds the unit cell of the simulation supercell.

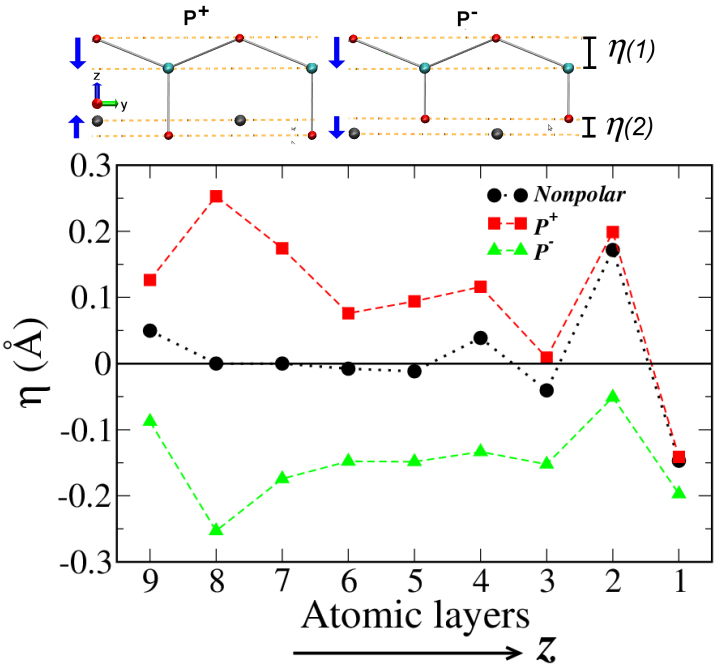

Figure 2. Out-of-plane atomic displacement η of a clean TiO_2-terminated (001) surface, defined as the cation-anion splitting $\eta = z_{cation} - z_{anion}$, for the nonpolar and polar P^+ and P^- PTO. Top panel: schematic atomic displacements with the arrows indicating the η direction at the first and second atomic layers ($\eta(1)$ and $\eta(2)$) for the P^+ and P^- cases.

$c_0 = 4.216$ Å is the PBE-sol out-of-plane lattice parameter of bulk PTO. Figure 2 shows the out-of-plane structural distortions as a function of the atomic layers for the three cases. In all of them, a superficial atomic rumpling with the oxygen atoms displaced outward against the deepest Ti atoms is observed (schematically shown in the top panel for the polarized surfaces), which is equivalent to an inward dipole in agreement with previous first-principles results [31, 32]. Note that neither surface reconstruction nor rotations of the oxygen octahedra are permitted.

Concerning the nanoribbon, a $zGNR$ with zigzag edges passivated with hydrogen atoms is considered. It is modeled using a primitive unit cell with 8 carbon atoms between edges in the non-periodic direction (y axis) as marked in Figure 1(b), and PBE-sol lattice parameter $a^o_{gr} = 2.459$ Å in the periodic direction (x axis). This unit is repeated three times in x-direction to build the simulation supercell which has a total of 24 C and 6 H atoms. In order to fit the nanoribbon over the in-plane ferroelectric supercell which is constituted by 2×4 a_{PTO} unit cells, we match and fix $3a_{gr}$ with $2a_{PTO}$ along x-direction. As a result, the nanoribbon is expanded by 5 % in that direction (strained $a_{gr} = 2.583$ Å), and compressed -4.52 % along y-direction. We have checked that this imposed strain does not affect the $zGNR$ band structure qualitatively (see Figure S2).

3. Results and Discussion

We begin by describing the most energetically stable structural arrangement of a $zGNR$ over the surface of a PTO monodomain with polarization P^+ and P^- and also in the nonpolar state. The results correspond to the combined system under the following structural constraints. The atomic positions of the PTO film and the Pt electrode hold those of the clean surface, while the $zGNR$ is kept flat and rigid under the strain described above. A total-energy mapping is performed by displacing iteratively the $zGNR$ (i) on the (001) plane and (ii) along the [001] direction, which allows to determine the optimized location and equilibrium distance d_{eq} to the TiO_2-terminated clean surface.

Previous DFT calculations for adatom adsorption on graphene [33] have shown that for atomic species of transition metals such as Ti, which is of our particular interest, the adatom is preferentially adsorbed on a *Hollow-site*, whereas for nonmetallic elements such as O, it is adsorbed at a *Bridge-site*. In the case of adsorption on a nanoribbon, the Ti atoms at a *H-site* have larger binding energy when they are located at the edges than in similar sites at the center of the $zGNR$, suggesting that the edges will have a significant contribution to the binding of $zGNR$ with a TiO_2 surface. Then, it is expected that in our system the location of the $zGNR$ will be a tradeoff between those atomic preferences on the TiO_2 surface and the structural constraint described before. In agreement with that, the $zGNR$ accommodates in order to equilibrate mainly the preferences of the C atoms with the Ti atoms which results in all the Ti atoms below the ribbon, close or exactly under *H-sites* as seen in Figure 1(b).

To determine the strength of the interaction $zGNR$-PTO, we compute the interaction energy E^{int} defined as

$$E^{int} = E^{zGNR/PTO/Pt} - (E^{zGNR} + E^{PTO/Pt}) \tag{1}$$

the total-energy difference between the hybrid system $zGNR/PTO/Pt$ and the separated systems: a freestanding $zGNR$ under the same strain conditions and the PTO/Pt system at the same atomic positions. Table 1 lists the interaction energy per $zGNR$ area unit (defined between H atoms at opposite edges and 3 a_{gr}), and d_{eq} for the lowest-energy configurations. When the PTO is polarized, we find that the adsorption increases compared to the nonpolar case, evidenced in the higher E_{int}'s but the d_{eq}'s to the PTO surface are practically similar. In turn, between polarized states, the $zGNR$ adsorption on the P^+ surface is hardly stronger than on the P^- surface. These d_{eq}'s are similar to the reported distances of graphene over others oxides, such as TiO_2 [25] and HfO_2 [34], but larger than the typical d_{eq} of atomic Ti and O on graphene sheets [33] driven by chemisorption. Based on that, we can speculate that the interaction $zGNR$-PTO is more of the physisorption type. In addition, our results indicate that the adsorption of $zGNR$ on PTO surface is ruled by the van der Waals interaction. When the calculations are performed without accounting for it, the $zGNR$-PTO interaction is much weaker as detailed in Table 1.

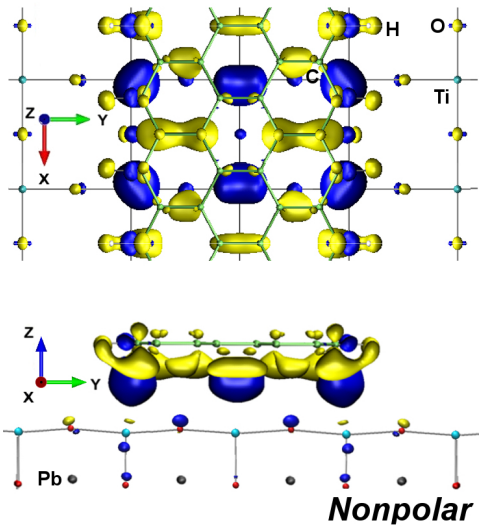

Figure 3. (Color online) Difference of electronic charge distribution at the interface of $zGNR$ over nonpolar PTO. The charge increase (loss) is shown in blue (yellow). Top and lateral view in the top and bottom panel, respectively. The $zGNR$ is plotted in green and the PTO atomic positions are marked only at the first atomic layer. Maps are plotted for an isosurface of 0.005 $e/\text{Å}^3$. Note that in the lateral view, the distribution for an unique row of Ti-O-Ti atoms is shown whilst it not the case for the $zGNR$.

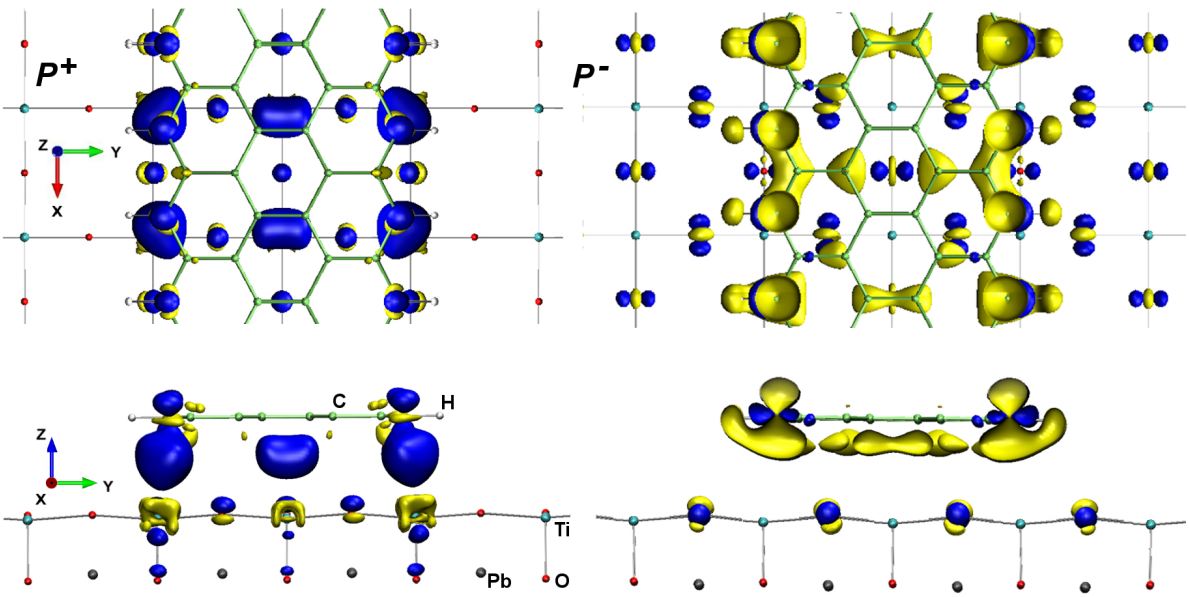

Figure 4. (Color online) Difference of electronic charge distribution at the interface of $zGNR$ over up-polarized (left panels) and down-polarized (right panels). Details idem to 3, except that here maps correspond to isosurfaces of 0.01 $e/\text{Å}^3$.

Table 1. Equilibrium distances d_{eq} and interaction energy of the $zGRN$ on the PTO film: nonpolar and polarized P^+ and P^- with constrained values of $|P| = 0.53\ P_0 = 42\ \mu C/cm^2$. The numbers between parenthesis were obtained without accounting for the van der Waals interaction.

PTO	d_{eq} (Å)	E_{int} (meV/Å^2)
nonpolar	3.05 (3.25)	-25.9 (-4.0)
P^+	2.95 (3.11)	-31.1 (-9.1)
P^-	3.00 (3.18)	-30.2 (-9.0)

Now to get insights about the interaction, we visualize the change in the electronic charge distribution obtained as follows.

$$\Delta n(\vec{r}) = n(\vec{r})_{zGNR/PTO/Pt} - [n(\vec{r})_{zGNR} + n(\vec{r})_{PTO/Pt}] \tag{2}$$

where $n(\vec{r})_{zGNR/PTO/Pt}$ is the charge density of the hybrid system, and the other terms correspond to the isolated components. Figures 3 and 4 show the $\Delta n(\vec{r})$ maps for the $zGNR$ on the nonpolar and polar PTO, respectively. We observe in all cases that the charge redistribution takes place in the region between the PTO surface and the $zGNR$ especially at its edges. It originates mainly by the interaction between the electronic cloud of the Ti and O atoms on the surface and the π electrons of the $zGNR$. When PTO is nonpolar (Figure 3), there is an important change in the charge density of the $zGNR$ with respect to a freestanding one: the carbon atoms closer to the Ti atoms present charge gain (blue lobes) displaced towards the center of the interface, whilst the carbons closer to the O atoms show charge loss (yellow lobes) just below them. In the edge C atoms, those changes appear also around them. In the Ti and O atoms on the PTO surface, minor changes are observed relative to those on a clean surface with deficiency and excess of charge, respectively, at the interface side. Note this redistribution is low compared with that in the polar cases (Figure 4) since the isosurface value here is one half of that used there. For each PTO polar state, only one of the features described for nonpolar PTO will be enhanced while the other one will fully disappear. This is, for the P^+ surface shown in Figure 4 (left), the electron transfer from the Ti to the C atoms is intensified depending notably on the carbon positions at the $zGNR$. In consistency with the high reactivity of the edges, $\Delta n(\vec{r})$ increases below and above the edge C atoms, whereas the increment only occurs in between the Ti atoms interacting with two C atoms in the $zGNR$ interior. For the P^- surface (Figure 4 right), the carbon atoms donate electrons (yellow regions) to the oxygen atoms on the surface, and again the edge carbon atoms present major changes. Finally, it is convenient to note that although the three PTO polarized states present similar atomic displacements at the surface, the electronic distribution is indeed different.

A condensed way to visualize such charge redistribution and movement of electrons towards or away from the $zGNR$, is to average $\Delta n(\vec{r})$ per xy-plane parallel to the surface. A charge density difference per unit length normal to the surface $\Delta n(z)$ is obtained and plotted in Figure 5. For the adsorption on the nonpolar surface, a nearly

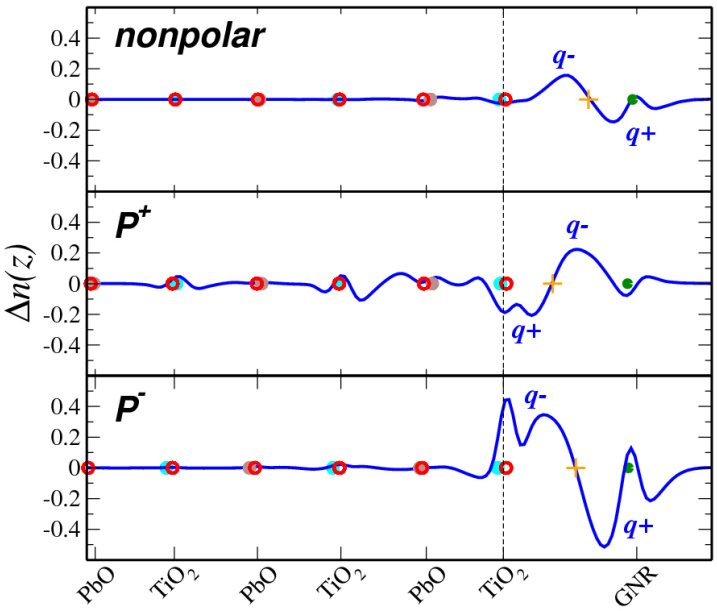

Figure 5. (Color online) Plane-average electron density difference $\Delta n(z)$ per unit length along z for the GRN adsorbed on the PTO surface nonpolar, and polarized P^+ and P^-. Cyan, brown, red and green circles denote Ti, Pb, O and $zGNR$ positions, respectively. The node z_0, marked with a cross, indicates where the charge difference vanishes between the surface and the $zGNR$. q^+ and q^- mean addition and removal of electrons, respectively.

symmetric separation happens exclusively at the interface noting in particular that there is no change at the PTO surface. Contrary, when the PTO is polarized a difference appears on the ferroelectric surface which clearly manifests the charge transfer towards the $zGNR$ from the P^+ surface and vice versa for the P^-. The charge q gained or lost per $zGNR$ atom can be quantified by integrating $\Delta n(z)$ arbitrarily [23] from the node z_0 located in the region in between both systems and the infinite

$$q = -e \int_{z_0}^{\infty} dz \; \Delta n(z)/N_{zGNR} \tag{3}$$

where N_{zGNR} is the total number of C and H atoms in the simulation cell, and $-e$ the charge of one electron. The computed charges q are 0.016 e and -0.007 e for $zGNRs$ adsorbed on the P^- and P^+ polarized surfaces, respectively, whose signs agree with the loss and gain of charge per $zGNR$ atom. In the nonpolar case, q is 0.004 e and comes mainly from the carbon atoms which showed charge loss just below the $zGNR$ but above the node z_0. Thus we note that the charge transferred towards the $zGNR$ increases almost linearly with the substrate positive polarization (later q will be plotted on the top axis in Figure 8 as proportional to the P indicated on the bottom axis, and extrapolating, the sign change will occur around $P \sim 14\mu C/cm^2$ as marked by the dashed line in that Figure). These charge values would help to explain why P^- can induce p-type doping in $zGNR$ whilst the symmetric P^+ is unable to induce n-type doping, as we will see below. Note also that the obtained charge values are similar to the

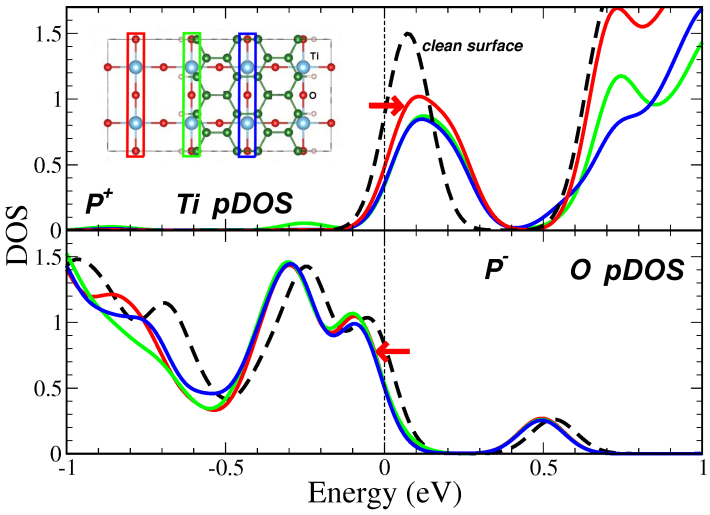

Figure 6. (Color online) Projected DOS on the Ti atoms at the polarized P^+ surface (top panel) and on the O atoms at the P^- surface (bottom panel). Dashed lines correspond to the atoms at the clean surface and color filled ones refer to the atoms enclosed by the respective rectangles.

calculated ones for graphene over anatase [26], and graphene physisorbed on different metal surfaces [23].

In order to analyze the $zGNR$ effect on the PTO, projected DOS over the surface atoms mainly involved in the interaction, i.e., Ti atoms on the P^+ surface and oxygen atoms on the P^- one, are plotted in Figure 6. For the P^+ clean surface, the Ti $3d$ states which contribute to the bottom of the conduction band (CB), are involved in the electronic reconstruction by receiving electrons from the Pt electrode and consequently cross the Fermi level towards lower energies (dashed line in the top panel). These atoms provide the charge to screen the depolarizing field of the imposed P^+. When the $zGNR$ is adsorbed, the transferred charge from the Ti to the C atoms is reflected in the shifting of the Ti $3d$ states towards higher energies as pointed by the arrow. Note that the projected DOS on the different Ti atoms (enclosed by different rectangles), those under the $zGNR$ and outside it, are shifted [35]. At the P^- polarized surface (bottom panel), the oxygen atoms are responsible of both passivating the surface charge of the polarization on the clean surface (also by electronic reconstruction, but holes move from the Pt electrode) and accepting charge from the C atoms when the $zGNR$ is adsorbed. Thus the O $2p$ states that determine the top of the valence band (VB), first cross the Fermi level to higher energies and then displace to lower ones.

3.0.1. Electronic structure changes in $zGNR$ To identify the changes on the $zGNR$ electronic structure induced by the ferroelectric polar states, the spin-polarized band structure of the hybrid system $zGNR$/PTO/Pt is computed. The site-projected wavefunction character of each band is calculated by projecting the wavefunctions onto spherical harmonics that are non-zero within spheres around each atom. Then we select

and add up the projections on all C and H atoms which form the $zGNR$. Figure 7 displays only the $zGNR$-atom projected band structure around the Fermi level for the three PTO polar states [36]. In the three cases, the α and β-spin states remain degenerated in all energy bands. On the nonpolar PTO surface, the band structure projected onto the $zGNR$ atoms looks similar to the freestanding strained case (see Figure S2) and the band gaps differ in less than 0.1 eV. When the ferroelectric substrate is polarized, new features show up. For adsorption on the P^+ surface, the whole band structure is shifted downward in energy. The bottom of CB and the top of the VB both fall approximately 0.4 eV and 0.1 eV compared to the nonpolar case, and the direct band gap narrows to approximately 0.11 eV. However, the bottom of the CB does not achieve to cross the Fermi level keeping the $zGNR$ *intrinsic* although close to n-type doping. When the PTO surface is polarized P^-, the top of the VB and the bottom of the CB are close to each other, and the top of the VB shifts ~ 0.2 eV above the Fermi level. The filled $zGNR$ electronic states become empty which results p-type doping. For comparison, Table 2 summarizes the calculated energy gap of a $zGNR$ under different conditions of adsorption and strain.

Table 2. Δ_z^0 and Δ_z^1 label the energy gap and the energy splitting at the X point of $zGNR$ under different strain and adsorption conditions. Notation and numbers between parenthesis follow ref. [12].

$zGNR$	Δ_z^0 (eV)	Δ_z^1 (eV)
Free, unstrained	0.50	0.60
	(0.33)	(0.50)
Free, strained	0.50	0.65
Strained on nonpolar	0.41	0.59
Strained on P^+	0.11	0.17
Strained on P^-	0.18	0.20

We notice that the constraint without structural relaxation on the PTO surface after the $zGNR$ adsorption (at the PTO surface, the oxygen atoms are always raised above the Ti atoms, while the $zGNR$ is kept plane) might be affecting the observed doping and needs further study. This is, on the P^+ surface the lower Ti atoms do not attain to dope n-type the $zGNR$, whereas on the P^- surface the more exposed O atoms are able to stabilize holes in $zGNR$ making it p-type. Furthermore the type of TiO_2 surface termination might also be contributing to the higher $zGNR$ electronic doping when adsorbed on the P^- surface.

3.0.2. Local magnetic properties of the zGNR We now analyze how the electronic charge transfer from the ferroelectric surface affects the stability of the local magnetic properties of the $zGNR$ especially at its edges. It is known that a freestanding $zGNR$ shows ferromagnetic coupling of spins along the ribbon edges and antiferromagnetic

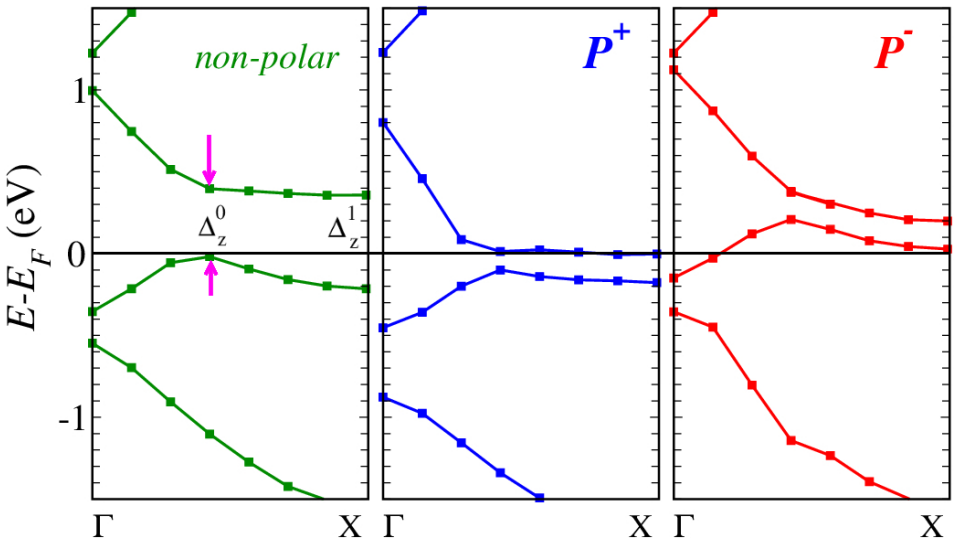

Figure 7. Hybrid-system electronic band structure projected onto the $zGNR$ atoms when it is adsorbed on the PTO surface with different polar states. The α and β-spin states are degenerate in all energy bands. Results are obtained using a 1×3 supercell as marked in Figure 1. The bands are downfolded three times with respect to those plotted on Figure S2.

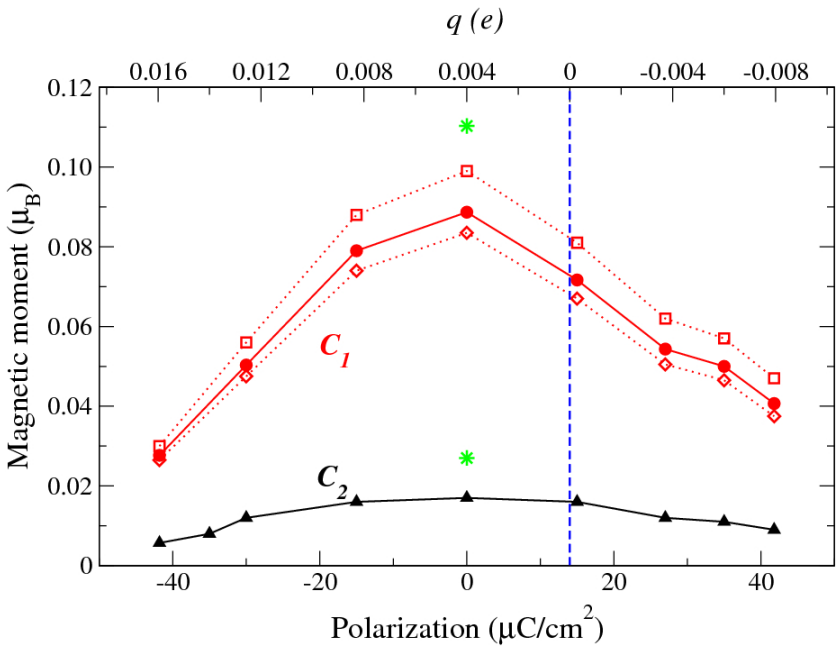

Figure 8. (Color online) Modulus of the magnetic moment per carbon atom at the edge (C_1) and its neighbor (C_2) in the AFM ground state as a function of the ferroelectric substrate polarization. Open symbols correspond to C_1 atoms above O atoms (squares) and above Ti atoms (diamonds). Stars indicate values for a freestanding $zGNR$. The top axis indicates the average amount of charge transferred per $zGNR$ atom obtained using Equation 3.

coupling between the two magnetic edges Besides the local magnetic moments of the carbon atoms decay exponentially as they enter into the ribbon interior [12]. When the $zGNR$ is adsorbed on the PTO surface, we find that the AFM ground state is preserved for the three polarized cases. However, the ferroelectric polarization can override that magnetic character. To demonstrate that, the local magnetic moments of the edge carbon atoms (C_1 and C_2 as labeled in Figure 1) are plotted in Figure 8 for different substrate polarization values in between P^- and P^+. When the ribbon is adsorbed on paraelectric PTO ($P = 0$), the magnetic moment per edge carbon atom is reduced from the pristine value in the freestanding counterpart (star symbols). For C_1 in particular, the average value decreases to 0.08 μ_B from 0.11 μ_B. In turn, the ferroelectric substrate polarization in both directions decreases even more the local magnetic moments of all carbon atoms. Such reduction can be attributed to the aforementioned charge transfer. This is, the edge carbon p_z states are filled when the $zGNR$ is adsorbed on the P^+ surface whilst are emptied on the P^- surface, as was quantified by the average charges plotted on the top axis, resulting in a local magnetization reduction in both cases. Also related to that, the local magnetic moments of the edge C_1 atoms depend on the adsorption site: those on-top of Ti atoms are smaller than those on O atoms.

In conclusion, using density functional theory we have studied the effect produced by the out-of-plane ferroelectric polarization of a PTO film on the electronic and magnetic properties of a nanosized graphene nanoribbon. The study has considered in detail the superficial rumpling of a pristine PTO surface but keeping the atomic positions of the unreconstructed surface and also the structural constraint of a flat nanoribbon. When the nanoribbon was adsorbed on the PTO surface, a charge transfer occured preferentially at the edges of the $zGNR$. For the surface polarized P^-, the whole band structure of the nanoribbon was up-shifted above the Fermi level showing p-type doping, whereas it was down-shifted when the surface was polarized P^+ but without crossing the Fermi level, in agreement with the charge distribution observed at the interface. We have also found that for both PTO polarization directions, the band gap of the adsorbed graphene nanoribbon narrowed to $\sim$ 0.1 eV when the surface polarization was approximately one half of the bulk value, compared to 0.4 eV when adsorbed on the nonpolar surface. The present theoretical results will help to provide correct interpretation of the normal-polarization intrinsic effect on a $zGNR$. The given atomic level details of the particular interface $PbTiO_3$ - nanoribbon can be useful considering the wide variety of recent works combining graphene with PZT for FETs.

The authors acknowledge support from CONICET-Argentina and the Universidad Nacional del Litoral for grant CAI+D 00471-2011. G D B thanks CONICET-Argentina for the Ph.D. fellowship.

References

[1] Geim A K and Novoselov K S 2007 *Nat. Mater.* **6** 183-191
[2] Jie W and Hao J 2014 *Nanoscale* **6** 6346-6362
[3] Hong X, Hoffman J, Posadas A, Zou K, Ahn C H and Zhu J 2010 *Appl. Phys. Lett.* **97** 033114
[4] Song E B, Lian B, Min K *et al* 2011 *Appl. Phys. Lett.* **99** 042109
[5] Rajapitamahuni A, Hoffman J, Ahn C H and Hong X 2013 *Nano Lett.* **13** 4374-4379
[6] Yusuf M H, Nielsen B, Dawber M and Du X 2014 *Nano Lett.* **14** 5437-5444
[7] Baeumer C, Rogers S P, Xu R, Martin L W and Shim M 2013 *Nano Lett.* **13** 1693-1698
[8] Zheng Y, Ni G-X, Toh C-T, Zeng M-G, Chen S-T, Yao K and Özyilmaz B 2009 *Appl. Phys. Lett.* **94** 163505
[9] Hong X, Zou K, DaSilva A M, Ahn C H and Zhu J 2012 *Solid State Commun.* **152** 1365-1374
[10] Baeumer C, Saldana-Greco D, Martirez J M P, Rappe A M, Shim M and Martin L W 2015 *Nature Comm.* **6** 6136
[11] Bischoff D, Varlet A, Simonet P, Eich E, Overweg H C, Ihn T and Ensslin K 2015 *Appl. Phys. Rev.* **2** 031301
[12] Son Y-W, Cohen M L and Louie S G 2006 *Phys. Rev. Lett.* **97** 216803
[13] Li Y Y, Chen M X, Weinert M and Li L 2014 *Nat. Commun.* **5** 4311
[14] Li X, Wang X, Zhang L, Lee S and Dai H 2008 *Science* **319** 1229-1232
[15] Wang X, Li X, Zhang L, Yoon Y, Weber P K, Wang H, Guo J and Dai H 2009 *Science* **324** 768-771
[16] Ding J, Wen L-W, Li H-D, Kang X-B and Zhang J-M 2013 *Eur. Phys. Lett.* **104** 17009
[17] Lee Y-L, Kim S, Park S, Ihm J, and Son Y-W 2010 *ACS Nano* **4** 1345-1350
[18] Kresse G and Hafner J 1993 *Phys. Rev. B* **47** 558(R) Kresse G and Furthmuller J 1996 *Phys. Rev. B* **54** 11169
[19] Perdew J P, Ruzsinszky A, Csonka G I, Vydrov O A, Scuseria G E, Constantin L A, Zhou X and Burke K 2008 *Phys. Rev. Lett.* **100** 136406
[20] Grimme S, Jens A, Ehrlich S and Krieg H 2010 *J. Chem. Phys.* **132** 154104
[21] This value is close to that of $SrTiO_3$ as it is known experimentally [22] when it is used as substrate, it fixes the PTO polarization to lie in the z direction.
[22] Venkatesan S, Vlooswijk A, Kooi B J, Morelli A, Palasantzas G, DeHosson J T M and Noheda B 2008 *Phys. Rev. B* **78** 104112
[23] Khomyakov P A, Giovannetti G, Rusu P C, Brocks G, van den Brink J and Kelly P J *Phys. Rev. B* **79** 195425
[24] Hsu A L, Koch R J, Ong M T, Fang W, Hofmann M and Kim K K 2014 *ACS Nano* **8** 7704-7713
[25] Gao H, Li X, Lv J and Liu G 2013 *J. Phys. Chem. C* **117** 16022-16027
[26] Mogilevsky G, Hartman O, Emmons E D, Balboa A, DeCoste J B, Schindler B J and Karwacki C J 2014 *ACS Applied Materials and Interfaces* **6**(13) 10638-10648
[27] Highland M J , Fister T T, Fong D D, Fuoss P H, Thompson C, Eastman J A, Streiffer S K and Stephenson G B 2011 *Phys. Rev. Lett.* **107** 187602
[28] Bungaro C and Rabe K M 2005 *Phys. Rev. B* **71** 035420
[29] Bengtsson L 1999 *Phys. Rev. B* **59** 12301
[30] Stengel M, Aguado-Puente P, Spaldin N A and Junquera J 2011 *Phys. Rev. B* **83** 235112
[31] Meyer B and Vanderbilt D 2001 *Phys. Rev. B* **63** 205426
[32] Piskunov S, Kotomin E A, Heifets E, Maier J, Eglitis R I and Borstel G 2005 *Surf. Sci.* **515** 75-88
[33] Nakada K and Ishii A 2011 *Graphene Simulation*, Prof. Jian Gong (Ed.) ISBN: 978-953-307-556-3, InTech
[34] Scopel W L, Fazzio A, Miwa R H and Schmidt T M 2013 *Phys. Rev. B* **87** 165307
[35] In a much broader supercell, it is expected that the Ti atoms far away from the $zGNR$ will behave similar as those in the clean surface. This was observed using a testing supercell of 2×7 unit cells in the plane.
[36] Bandstructure graphics were done using the p4vasp program http://www.p4vasp.at/